THE DEVELOPMENT AND TESTING OF A DAM-BREAK FLOOD FORECASTING MODEL

By D. L. Fread, Research Hydrologist, Hydrologic Research Laboratory, W23, Office of Hydrology, National Weather Service, NOAA, Silver Spring, Maryland 20910.

ABSTRACT

The theoretical aspects of a mathematical model to forecast the flood hydrograph resulting from a breached dam are presented. The model is composed of two basic elements. The first simulates the outflow hydrograph due to a time-dependent, erosion-type breach of a dam using a hydraulic weir representation of the outflow through the breach while simultaneously considering the effects of the reservoir storage depletion and the inflow hydrograph via either a storage or dynamic routing technqiue. The second element routes the generated outflow hydrograph through the downstream valley via an implicit finite difference solution of the complete one-dimensional equations of unsteady flow. Essential input data consists of: (1) the geometrical and temporal description of the breach, (2) the reservoir depth, length, and either storage-elevation or top width-elevation tables, and (3) the Manning roughness coefficient-elevation and top width-elevation tables for the downstream valley. A minimal number of tables can be specified since the numerous computational sections required in the finite difference solution of rapidly varying dam-break waves are generated within the model via interpolation. The model is applied to the dam-break floods which resulted from the failures of the Teton Dam and the Buffalo Creek coal-waste dam to test its ability to reconstitute observed downstream peak stages, discharges, and travel times. Simulation accuracy, computer requirements, input parameter sensitivities, and numerical computational characteristics are presented for each of the applications.

INTRODUCTION

The National Weather Service (NWS) has the responsibility to advise the public of downstream flooding when there is a failure of a dam having an impoundment of water. Although this type of flood has many similarities to floods produced by precipitation runoff (the latter being the type of flood that the NWS has over the years developed the technology and expertise to forecast), the dam-break flood has some very important differences which make it difficult to analyze with the common techniques which have worked so well for the precipitation-runoff floods. This situation was recently recognized when the Teton Dam failed and the NWS River Forecast Center (RFC) in Portland had the responsibility for providing flood warnings (expected peak stages, discharges, and times of occurrence) for communities of the Teton-Snake River Valley downstream of the Teton Dam.

The potential for catastrophic flooding due to dam failures has recently been brought to the Nation's attention by several dam failures such as the Buffalo Creek coal-waste dam, the Rapid City Dam, the Teton Dam, and the Johnstown Dam. A report by the U.S. Department of the Army [1975] gives an inventory of the Nation's approximately 49,000 dams with heights greater than 25 feet or storage volumes in excess of 50 acre-feet. The report also classifies some 20,000 of these as being "so located that failure of the dam could result in loss of human life and appreciable property damage ...." The NWS considers the dam-break problem of sufficient importance to commence a program for the development of a flood forecast procedure especially designed to cope with the unique characteristics of dam-break floods.

In general, the forecasting of a dam-break flood consists of three parts; namely: (1) estimation of the mode of failure, i.e., the temporal and geometrical description of the breach (opening in the dam through which the impounded water escapes into the downstream valley); (2) computation of the outflow discharge hydrograph produced by the breach, including effects such as reservoir inflow and spillway and/or turbine outflows; and (3) routing of the outflow hydrograph through the downstream valley in order to determine the hydrograph modifications, the resulting water surface elevations (stages), and the flood-wave travel times.

Some general requirements of a dam-break flood forecasting model are considered to be the following: (1) the model should be general with wide applicability; (2) it must be economically feasible to use in an operational environment, i.e., it must have practical computational requirements and it should require a reasonably small effort by the forecaster to specify the necessary data; (3) it should be able to function with various levels of input data ranging from rough estimates and even guesses to complete data specifications (the latter may occur when updating a forecast sometime after the failure has occurred and more data are available or when using the model for hindcasting for purposes of procedural development); (4) it must require data which are available or which require minimal effort by the forecaster to obtain; (5) the computational scheme should be robust, i.e., the computations do not easily "blow up" or become unstable; and (6) the model should be capable of simulating the most important characteristics of each of the three component parts of dam-break floods as outlined above.

This paper presents the theoretical development and limited testing of a dam-break flood forecasting model. Test applications include simulation of observed peak stages, discharges, and travel times associated with the catastrophic floods which resulted from the Teton Dam failure and the collapse of the Buffalo Creek coal-waste dam.

MODEL DEVELOPMENT

Breach Formation

The breach is the opening formed in the dam as it fails. The impounded waters escape through the breach into the valley downstream of the dam. Many investigators [Ritter, 1892; Schocklitsch, 1891; Ré, 1946; Dressler, 1954; Stoker, 1957; Su and Barnes, 1969; Sakkas and Strelkoff, 1973] of dam-break floods have assumed the breach is complete, i.e., it encompasses the entire dam; and they have assumed also that the breach is formed instantaneously. Others [Schocklitsch, 1891; Army Corps of Engineers, 1960, 1961] have recognized the need for partial, instantaneous breaches in which the geometry of the breach is rectangular, triangular, or trapezoidal. The assumption of instantaneous and complete breaches, while attractive for reasons of convenience when applying certain mathematical techniques for analyzing dam-break flood waves, is not generally the most appropriate assumption of the breach formation in many dam failures. This is particularly true of earth and rock-fill dams which require a finite interval of time for the breach to achieve its final form. Also, masonry dams may fail as a partial breach which forms rapidly with time but only approaching an instantaneous failure. The actual failure mechanics are not well understood for either earth or masonry dams. Some effort was made by [Cristofano, 1965] to better describe the breach formation geometrically and temporally for erosion failures of dams; however, this procedure also requires critical assumptions to be made.

For reasons of simplicity, generality, wide applicability, and the recognized uncertainty in the actual failure mechanism, the dam-break flood forecasting model developed herein assumes the breach is time-dependent with either rectangular, triangular, or trapezoidal shape. Such a breach can closely approximate those breaches which approach an instantaneous development. The variable geometry enables either partial or complete breaches to be simulated. The forecaster can specify the geometrical shape, size, and formation time with a minimum of parameters. This is most advantageous for updating or hindcasting when particular information of the breach development may be available from estimates by eye-witnesses or detailed surveys made after the event. Selection of parameter values before the breach forms or after it forms in the absence of any observation introduces a varying degree of uncertainty in the forecast model; however, as will be shown later, errors in the description of the breach formation and the resulting outflow hydrograph may be rapidly damped-out as the flood wave advances downstream.

The assumed breach is shown in Fig. 1. It is assumed to start at a specified elevation of the reservoir water surface (h_o) with an initial base width (b) which remains constant as the breach forms or enlarges via an erosion process at a constant rate from time $t=0$ to time $t=\tau$

when the breach reaches its final size and shape. The geometrical shape is controlled by the value assigned to b and by the parameter z which defines the side slopes of the breach, i.e., 1 vertical to z horizontal. The final size of the breach is controlled by the minimum elevation h_{bm} to which the bottom of the breach finally reaches. A useful value for tracking with time the breach formation is the instantaneous elevation of the breach bottom (h_b) which is given by the following expression:

$$h_b = h_{bm} + (h_o - h_{bm})\left(\frac{\tau - t}{\tau}\right) \qquad 0<t<\tau \quad \ldots\ldots\ldots\ldots \quad (1)$$

$$h_b = h_{bm} \qquad t \geq \tau \quad \ldots\ldots\ldots\ldots \quad (2)$$

Thus, in this paper, the time-dependent complete or partial breach of rectangular, triangular, or trapezoidal shape is described by five parameters (h_o, b, z, h_{bm}, τ).

Outflow Hydrograph

The outflow of the impounded waters through the breach is assumed to be best approximated by broad-crested weir flow. The outflow through the broad-crested weir is a function of the shape of the breach and the head on the weir. The shape can be either rectangular (z=0), triangular (b=0), or trapezoidal. The weir head is the difference between the instantaneous water surface elevation (h) at a location a short distance within the reservoir where drawdown effects are minimal and the instantaneous bottom elevation (h_b) of the breach or broad-crested weir given as a function of time by Eqs. (1-2). An expression for the instantaneous outflow (Q_b) through the breach is:

$$Q_b = c_1(h-h_b)^{1.5} + c_2(h-h_b)^{2.5} \qquad h>h_b \quad \ldots\ldots\ldots\ldots \quad (3)$$

where:

$$c_1 = 3.08\ b\ c_v\ c_s \quad \ldots\ldots\ldots\ldots \quad (4)$$

$$c_2 = 2.44\ z\ c_v\ c_s \quad \ldots\ldots\ldots\ldots \quad (5)$$

in which c_v is the correction due to the velocity of approach immediately upstream of the breach and c_s is the correction for submergence of broad-crested weirs. The term in Eq. (3) containing c_1 denotes the portion of weir flow through a rectangular weir of width b; the term with c_2 represents the portion of weir flow through a V-shaped weir as is the case if the breach is of triangular shape or the end portions

of a trapezoidal shaped breach. The velocity of approach correction c_v is approximated by the following expression [Brater, 1962]:

$$c_v = 1.0 + \frac{0.75\ v^2}{g(h'-h_b')} \quad \ldots\ldots\ldots\ldots\ldots\ldots\ldots\ldots \quad (6)$$

in which g is the acceleration due to gravity and the prime (') superscript on h and h_b denotes that these are evaluated at a slightly previous time, and v is given by:

$$v = \frac{Q_b'}{B_d\ h'} \quad \ldots\ldots\ldots\ldots\ldots\ldots\ldots\ldots\ldots\ldots \quad (7)$$

in which B_d is the vertically averaged width of the reservoir in the vicinity of the dam. The correction for the effects of submergence are necessary when the water surface elevation (h_d) of the flow downstream of the dam exceeds a value of about 0.67h. A submergence correction factor c_s for broad-crested weirs [Venard, 1958] is computed from the following:

$$c_s = 1.0 \qquad h_d'/h' < 0.67 \quad \ldots\ldots\ldots\ldots \quad (8)$$

$$c_s = 1.0 - 27.8(h_d'/h' - 0.67)^3 \qquad h_d'/h' > 0.67 \quad \ldots\ldots\ldots\ldots \quad (9)$$

in which the prime superscripts indicate that the submergence factor is evaluated at a slightly previous time when all elevations are known. The term h_d is the elevation of the water surface immediately downstream of the dam and is approximated from Manning's equation for a wide channel, i.e.,

$$h_d' = \left[\frac{Q_b'\ n_d}{1.49\ S_d^{0.5} B_d}\right]^{0.6} \quad \ldots\ldots\ldots\ldots\ldots\ldots\ldots\ldots \quad (10)$$

in which n_d is the Manning roughness coefficient, S_d is the average bottom slope of the river immediately downstream of the dam, and Q_b' and B_d are as previously defined.

The total instantaneous outflow (Q) from the dam is composed of the flow (Q_b) through the breach and the flow (Q_s) through the dam spillway(s), gates, and/or turbine discharges, and along the crest of the dam. The Q_s component is allowed to vary as the water surface elevation varies until it recedes below the spillway, gate, or dam crest elevations, i.e., h_s, h_g, and h_o, respectively. Thus, an expression for the total instantaneous flow (Q) is:

$$Q = Q_b + Q_s \quad \ldots\ldots\ldots\ldots\ldots\ldots\ldots\ldots\ldots\ldots \quad (11)$$

where:

$$Q_s = C_s(h'-h_s)^{3/2} + C_g a(h'-h_g)^{1/2} + C_d(h'-h_o)^{3/2} + Q_t \quad \ldots\ldots \quad (12)$$

in which C_s, C_g, and C_d are the discharge coefficients for the spillway, gates, and dam crest; and Q_t is the constant turbine discharge, and a is the gate area.

Since Q_b is a function of the reservoir water surface elevation (h), the depletion of the reservoir storage by the outflow (Q_b) causes a decrease in h which simultaneously causes a decrease in Q_b. However, any inflow to the reservoir tends to cause h and Q_b to increase. In order to determine the total reservoir outflow Q as a function of time, the simultaneous effects of reservoir storage depletion and inflow require the use of a reservoir routing technique. The forecasting model presented herein has the option to use two types of reservoir routing, namely: (1) a hydrologic storage routing technique or (2) a hydraulic dynamic routing technique. A discussion of the features of the latter will be delayed until after the downstream routing technique is presented.

The hydrologic storage routing technique is based on the law of conservation of mass or so-called storage equation, i.e.,

$$I - Q = dS/dt \quad \ldots\ldots\ldots\ldots\ldots\ldots\ldots\ldots \quad (13)$$

where I is the inflow during the differential time interval (dt), Q is the outflow during the same interval, and dS is the change in reservoir storage. The inflow (I) is a known function of time. The outflow Q is a function of h and h_b, the former an unknown function of time and the latter a known function of time as defined by Eqs. (1-2). Writing Eq. (13) in terms of finite differences yeilds:

$$\left(\frac{I+I'}{2}\right) - \left(\frac{Q+Q'}{2}\right) = \frac{\Delta S}{\Delta t} \quad \ldots\ldots\ldots\ldots\ldots\ldots\ldots \quad (14)$$

where the prime (') superscripts denote values at the time t-Δt and the Δ approximates the differential. Upon rearranging Eq. (14), the following is obtained:

$$\frac{2\Delta S}{\Delta t} + Q + Q' - I - I' = 0 \quad \ldots\ldots\ldots\ldots\ldots\ldots \quad (15)$$

where:

$$\Delta S = \left(\frac{A_s + A'_s}{2}\right)(h-h') \quad \ldots\ldots\ldots\ldots\ldots\ldots\ldots \quad (16)$$

in which A_s is the surface area of the reservoir and is a known function of h. Upon substituting Eqs. (3), (11), and (16) into Eq. (15), the following is obtained:

$$\frac{1}{\Delta t}(A_s+A_s')(h-h') + c_1(h-h_b)^{1.5} + c_2(h-h_b)^{2.5} + Q_s + Q' - I - I' = 0 \quad (17)$$

Since A_s is a function of h and A_s', h', c_1, h_b, c_2, Q_s, Q', I, and I' are known at time t, Eq. (16) can be solved for the unknown value of h using Newton-Raphson iteration. Once h is obtained, Eqs. (3) and (11) can be used to obtain the outflow (Q) at time (t). In this way, the outflow hydrograph can be developed for each time (t) as t goes from t=0 to some terminating time, say t_e. The advance in time is accomplished by taking Δt time steps which are assigned magnitudes relative to the time (τ) at which the breach achieves its maximum size and when the outflow usually achieves its maximum value. The Δt values are computed according to the following criteria which results in minimal numerical integration errors:

$$\Delta t = 0.02\tau \qquad t \leq \tau \quad (18)$$

$$\Delta t = 0.10\tau \qquad t > \tau \quad (19)$$

Downstream Routing

After determining the hydrograph of the outflow at the dam, the extent of flooding in the downstream valley is determined by routing the outflow hydrograph through the valley.

The hydrograph is modified as it is routed through the valley due to the effects of valley (channel) storage and frictional resistance. If the channel is rectangular, the reach length short, and the frictional resistance low, the hydrograph (flood wave) remains essentially unchanged and may be treated as uniformly progressive flow. However, if the rectangular channel is long and/or if the channel resistance is high, the flood wave will be modified appreciably as it moves through the channel. The modifications include attenuation of the flood peak, spreading-out or dispersion of the flood volume, and changes in the celerity (translation speed) or travel time of the flood. If the channel contains significant storage volume downstream of the dam, such as a gradual or sudden increase in channel (valley) width, the flood wave can be extensively attenuated and its time of travel greatly reduced.

A distinguishing characteristic of dam-break flood waves is the great magnitude of the peak discharge when compared to runoff-type floods which have occurred in the same valley. The dam-break flood is usually many times greater than the runoff flood of record. This results in much higher velocities associated with dam-break floods than other floods and causes an increase in the modifying effects due to cross-sectional expansions and contractions. Also, the above-record discharges of

the dam-break flood make it necessary to extrapolate certain coefficients used in various routing techniques and make it impossible to fully calibrate the routing technique.

Another distinguishing characteristic of dam-break floods is the very short time base and particularly the extremely short time from beginning of rise until the occurrence of the peak discharge. The time to peak may have values ranging from only a few minutes to usually no more than a few hours. This feature, coupled with the great magnitude of the peak discharge, causes the dam-break flood wave to have acceleration components of a far greater significance than those associated with floods generated by precipitation runoff. Thus, routing techniques which include acceleration effects are desirable for treating dam-break floods.

There are two basic types of flood routing, the hydrologic method and the hydraulic method. The hydrologic method is more of an approximation of the phenomena than the hydraulic method and is used for convenience and economy of computation. It is most appropriate as far as accuracy is concerned when the flood wave is not rapidly varying (acceleration effects are negligible) and when the flood wave is similar in shape and magnitude to previous floods for which observations of stage and discharge hydrographs are available for calibrating the necessary routing coefficients.

The hydraulic method is chosen for the downstream routing component of the dam-break flood forecasting model presented herein. This choice is based on its potential for providing a significant advantage in accuracy over the hydrologic method while requiring a very reasonable amount of computational effort by an IBM 360/195 computer, the machine available for NWS forecasters. Accuracy and computational effort will be discussed later when the results of testing the forecast model are presented.

Although there are also simplified hydraulic routing techniques such as kinematic or diffusion routing, they are not chosen because of the importance of the acceleration effects associated with dam-break floods and the relative insignificant savings in computational effort afforded by such simplifications. Instead, the dynamic routing technique is chosen.

Dynamic Routing.--This type of hydraulic routing technique is based on the complete one-dimensional equations of unsteady flow, whose original derivation is attributed to Barré de Saint-Venant [1871]. The applicability of the Saint-Venant equations to simulate abrupt waves such as the dam-break wave has been demonstrated by Terzidis and Strelkoff [1970] and by Martin and Zovne [1971].

The conservation form of the unsteady flow equations, in which the dependent variables are discharge (Q) and water surface elevation (h), consists of two equations. The first is based on the principle of conservation of mass and is:

$$\frac{\partial Q}{\partial x} + \frac{\partial (A+A_o)}{\partial t} - q = 0 \quad \ldots\ldots\ldots\ldots\ldots\ldots\ldots\ldots \quad (20)$$

where A is the active cross-sectional area of flow, A_o is the inactive (off-channel storage) cross-sectional area, x is the longitudinal distance along the channel, t is the time, and q is the lateral inflow or outflow per lineal distance along the channel (inflow is positive and outflow is negative). The second equation is based on the principle of conservation of momentum and is:

$$\frac{\partial Q}{\partial t} + \frac{\partial (Q^2/A)}{\partial x} + gA\left(\frac{\partial h}{\partial x} + S_f + S_{ce}\right) = 0 \quad \ldots\ldots\ldots\ldots\ldots\ldots \quad (21)$$

where g is the acceleration due to gravity, S_f is the friction slope, and S_{ce} is the expansion-contraction slope. The friction slope is evaluated herein from Manning's equation for uniform, steady flow, i.e.,

$$S_f = \frac{n^2 |Q| Q}{2.21\ A^2\ R^{4/3}} \quad \ldots\ldots\ldots\ldots\ldots\ldots\ldots\ldots \quad (22)$$

in which n is the Manning roughness coefficient and R is the hydraulic radius defined herein as A/B where B is the top width of the active cross-sectional area. The contraction-expansion slope is defined by the following:

$$S_{ce} = \frac{k\ \Delta V^2}{2g\ \Delta x} \quad \ldots\ldots\ldots\ldots\ldots\ldots\ldots\ldots \quad (23)$$

in which k is the expansion-contraction coefficient varying from 0.0 to 1.0 (positive if contraction and negative if expansion), ΔV^2 is the difference between the square of the velocities at two adjacent cross-sections separated by a distance, Δx. The lateral inflow (outflow) term (q) is not included in Eq. (21) since in this paper the lateral flow is assumed to enter or exit with no velocity component in the x-direction.

Eqs. (20-21) constitute a system of partial differential equations of the hyperbolic type. They contain two independent variables, x and t, and two dependent variables, h and Q; the remaining terms are either functions of x, t, h, and/or Q, or they are constants. These equations are not amenable to analytical solutions except in cases where the channel geometry and boundary conditions are uncomplicated and the non-linear properties of the equations are either neglected or made linear. The equations may be solved numerically by performing two

basic steps. First, the partial differential equations are represented by a corresponding set of finite difference algebraic equations; and second, the system of algebraic equations is solved in conformance with prescribed initial and boundary conditions.

Numerical Solution.--Eqs. (20-21) can be solved by either explicit or implicit finite difference techniques [Liggett and Cunge, 1975]. Explicit methods, although simpler in application, are restricted by mathematical stability considerations to very small computational time steps (on the order of a few minutes). Such small time steps cause the explicit methods to be very inefficient in the use of computer time. Implicit finite difference techniques [Preissmann, 1961; Amein and Fang, 1970; Strelkoff, 1970], however, have no restrictions on the size of the time step due to mathematical stability; however, convergence considerations may require its size to be limited [Fread, 1974a].

Of the various implicit schemes that have been developed, the "weighted four-point" scheme first used by Preissmann [1961] and recently by Chaudhry and Contractor [1973] and Fread [1974b] appears most advantageous since it can readily be used with unequal distance steps and its stability-convergence properties can be controlled easily. In the weighted four-point implicit finite difference scheme, the continuous x-t region in which solutions of h and Q are sought is represented by a rectangular net of discrete points. The net points are determined by the intersection of lines drawn parallel to the x and t axes. Those parallel to the x axis represent time lines; they have a spacing of Δt, which need not be constant. Those parallel to the t axis represent discrete locations or nodes along the river (x axis); they have a spacing of Δt, which also need not be constant. Each point in the rectangular network can be identified by a subscript (i) which designates the x position and a superscript (j) which designates the time line.

The time derivatives are approximated by a forward difference quotient centered between the i^{th} and i+1 points along the x axis, i.e.,

$$\frac{\partial K}{\partial t} \simeq \frac{K_i^{j+1} + K_{i+1}^{j+1} - K_i^j - K_{i+1}^j}{2\,\Delta t_j} \quad \ldots\ldots\ldots\ldots\ldots\ldots \quad (24)$$

where K represents any variable.

The spatial derivatives are approximated by a forward difference quotient positioned between two adjacent time lines according to weighting factors of θ and $1-\theta$, i.e.,

$$\frac{\partial K}{\partial x} \simeq \theta \left[\frac{K_{i+1}^{j+1} - K_i^{j+1}}{\Delta x_i}\right] + (1-\theta) \left[\frac{K_{i+1}^j - K_i^j}{\Delta x_i}\right] \quad \ldots\ldots\ldots\ldots\ldots \quad (25)$$

Variables other than derivatives are approximated at the time level where the spatial derivatives are evaluated by using the same weighting factors, i.e.,

$$K \simeq \theta \left[\frac{K_i^{j+1} + K_{i+1}^{j+1}}{2}\right] + (1-\theta) \left[\frac{K_i^{j} + K_{i+1}^{j}}{2}\right] \quad \ldots\ldots\ldots\ldots\ldots \quad (26)$$

A θ weighting factor of 1.0 yields the fully implicit or backward difference scheme used by Baltzer and Lai [1968]. A weighting factor of 0.5 yields the box scheme used by Amein and Fang [1970]. The influence of the θ weighting factor on the accuracy of the computations was examined by Fread [1974a], who concluded that the accuracy decreases as θ departs from 0.5 and approaches 1.0. This effect becomes more pronounced as the magnitude of the computational time step increases. In this paper, a weighting factor of 0.60 is used so as to minimize the loss of accuracy associated with greater values while avoiding the possibility of a weak or pseudo instability noticed by Baltzer and Lai [1968, Chaudhry and Contractor [1973].

When the finite difference operators defined by Eqs. (24-26) are used to replace the derivatives and other variables in Eqs. (20-21), the following weighted four-point implicit difference equations are obtained:

$$\theta \left[\frac{Q_{i+1}^{j+1} - Q_i^{j+1}}{\Delta x_i}\right] - \theta\, q_i^{j+1} + (1-\theta)\left[\frac{Q_{i+1}^{j} - Q_i^{j}}{\Delta x_i}\right] - (1-\theta)\, q_i^{j}$$

$$+\left[\frac{(A+A_o)_i^{j+1} + (A+A_o)_{i+1}^{j+1} - (A+A_o)_i^{j} - (A+A_o)_{i+1}^{j}}{\Delta t_j}\right] = 0 \quad \ldots\ldots\ldots \quad (27)$$

$$\left[\frac{Q_i^{j+1} + Q_{i+1}^{j+1} - Q_i^{j} - Q_{i+1}^{j}}{\Delta t_j}\right] + \theta\left[\frac{(Q^2/A)_{i+1}^{j+1} - (Q^2/A)_i^{j+1}}{\Delta x_i}\right.$$

$$\left. + g\,\bar{A}^{j+1}\left[\frac{h_{i+1}^{j+1} - h_i^{j+1}}{\Delta x_i} + \bar{S}_f^{j+1} + S_{ce}^{j+1}\right]\right] + (1-\theta)\left[\frac{(Q^2/A)_{j+1}^{j} - (Q^2/A)_i^{j}}{\Delta x_i}\right.$$

$$\left. + g\,\bar{A}^{j}\left[\frac{h_{i+1}^{j} - h_i^{j}}{\Delta x_i} + \bar{S}_f^{j} + S_{ce}^{j}\right]\right] = 0 \quad \ldots\ldots\ldots\ldots\ldots \quad (28)$$

where:

$$\bar{A} = (A_i + A_{i+1})/2 \quad \ldots \quad (29)$$

$$\bar{S}_f = n^2 \bar{Q}|\bar{Q}| / (2.2\, \bar{A}^2\, \bar{R}^{4/3}) \quad \ldots \quad (30)$$

$$\bar{Q} = (Q_i + Q_{i+1})/2 \quad \ldots \quad (31)$$

$$\bar{R} = \bar{A}/\bar{B} \quad \ldots \quad (32)$$

$$\bar{B} = (B_i + B_{i+1})/2 \quad \ldots \quad (33)$$

The terms associated with the j^{th} time line are known from either the initial conditions or previous computations. The initial conditions refer to values of h and Q at each node along the x axis for the first time line (j=1).

Eqs. (27-28) cannot be solved in an explicit or direct manner for the unknowns since there are four unknowns and only two equations. However, if Eqs. (27-28) are applied to each of the (N-1) rectangular grids between the upstream and downstream boundaries, a total of (2N-2) equations with 2N unknowns can be formulated. (N denotes the total number of nodes.) Then, prescribed boundary conditions, one at the upstream boundary and one at the downstream boundary, provide the necessary two additional equations required for the system to be determinate. The resulting system of 2N non-linear equations with 2N unknowns is solved by a functional iterative procedure, the Newton-Raphson method [Amein and Fang, 1970].

Computations for the iterative solution of the non-linear system are begun by assigning trial values to the 2N unknowns. Substitution of the trial values into the system of non-linear equations yields a set of 2N residuals. The Newton-Raphson method provides a means for correcting the trial values until the residuals are reduced to a suitable tolerance level. This is usually accomplished in one or two iterations through use of linear extrapolation for the first trial values. If the Newton-Raphson corrections are applied only once, i.e., there is no iteration, the non-linear system of difference equations degenerates to the equivalent of a quasi-linear difference formulation which may require smaller time steps than the non-linear formulation for the same degree of numerical accuracy.

A system of 2N x 2N linear equations relates the corrections to the residuals and to a Jacobian coefficient matrix composed of partial derivatives of each equation with respect to each unknown variable in that equation. The coefficient matrix of the linear system has a

banded structure which allows the system to be solved by a compact quad-diagonal Gaussian elimination algorithm [Fread, 1971], which is very efficient with respect to computing time and storage. The required storage is 2N x 4 and the required computational steps are approximately 38N.

Boundary Conditions.--The upstream boundary condition immediately downstream of the dam is the reservoir outflow hydrograph Q(t) which is computed as described in the previous section. This boundary condition is given by the following:

$$Q_1^{j+1} - Q(t) = 0 \quad \ldots\ldots\ldots\ldots\ldots\ldots\ldots\ldots \quad (34)$$

The downstream boundary condition is a stage-discharge relation for non-uniform, unsteady flow. It is expressed in terms of the Manning equation in which the friction slope S_f is evaluated by a backward difference approximation of Eq. (21) in which S_{ce} is assumed negligible. This boundary condition is given by the following:

$$Q_N^{j+1} - \frac{1.49}{n} A_N^{j+1} \left(A_N^{j+1}/B_N^{j+1}\right)^{2/3} S_f^{1/2} = 0 \quad \ldots\ldots\ldots\ldots \quad (35)$$

where:

$$S_f = -\left[\frac{h_N^j - h_{N-1}^j}{\Delta x_{N-1}}\right] - \left[\frac{Q_N^{j+1} - Q_N^j}{g\,\bar{A}\,\Delta t_j}\right] - \left[\frac{(Q^2/A)_N^j - (Q^2/A)_{N-1}^j}{g\,\bar{A}\,\Delta x_{N-1}}\right] \quad \ldots\ldots\ldots \quad (36)$$

in which:

$$\bar{A} = (A_{N-1}^j + A_N^j)/2 \quad \ldots\ldots\ldots\ldots\ldots\ldots\ldots\ldots \quad (37)$$

Eq. (35) reproduces the hysteresis effect in stage-discharge relations often observed as a loop-rating curve. The loop is produced by the effect of the acceleration and water surface slope terms in Eq. (21).

Initial Conditions.--The initial conditions represent the known or assumed values of Q and h for all nodes along the downstream channel. Steady flow is assumed as the initial condition with the discharge allowed to vary along the channel reach according to the following linear relationship:

$$Q_i^j = Q_1^j + (Q_N^j - Q_1^j)\frac{(x_i - x_1)}{(x_N - x_1)} \qquad \begin{matrix} j = 1 \\ i = 1, 2, \ldots N \end{matrix} \quad \ldots\ldots\ldots \quad (38)$$

where Q_N^j is the known or estimated discharge at the downstream boundary at time t=0, and x is the distance downstream of the dam. The initial water surface elevation (h_i^1) for each node is computed from Manning's equation for steady flow, normal depth conditions, i.e.,

$$Q_i^{j=1} - \frac{1.49}{n} \frac{A_i^{5/3}}{B_i^{2/3}} S_o^{1/2} = 0 \qquad i = 1, 2, \ldots N \quad \ldots\ldots\ldots \quad (39)$$

where S_o is bottom slope of the channel, A and B are known functions of the unknown water surface elevation (h). Eq. (39) is solved for h by Newton-Raphson iteration. An initial condition of $Q_i^1 > 0$ must be specified. Computational problems (of the form of computed depths which yield negative cross-sectional areas) are associated with the degree that Q_i^1 approaches a zero value.

Supercritical Flow.-The previous boundary conditions are applicable when the flow is subcritical, i.e., the velocity is less than the celerity of an infinitesimal gravity wave or,

$$V < \sqrt{gA/B} \quad \ldots\ldots\ldots\ldots\ldots\ldots\ldots\ldots\ldots\ldots \quad (40)$$

When the flow occurs in channels having very steep bottom slopes, it may become supercritical, i.e.,

$$V > \sqrt{gA/B} \quad \ldots\ldots\ldots\ldots\ldots\ldots\ldots\ldots\ldots\ldots \quad (41)$$

When the flow is supercritical, the theory of characteristics as applied to hyperbolic partial differential equations dictates the necessity for two upstream boundary conditions while eliminating the need for a downstream boundary condition. In addition to Eq. (34), a stage-discharge relation similar to Eq. (35) is used at the upstream boundary. This relation is based on the Manning equation for non-uniform, steady flow as follows:

$$Q_1^{j+1} - \frac{1.49}{n} A_1^{j+1} (A_1^{j+1}/B_1^{j+1})^{2/3} S^{1/2} = 0 \quad \ldots\ldots\ldots\ldots \quad (42)$$

where:

$$S = (h_1^j - h_2^j)/\Delta x_1 \quad \ldots\ldots\ldots\ldots\ldots\ldots\ldots\ldots \quad (43)$$

A modified compact quad-diagonal Gaussian elemination algorithm similar to the one previously described is required for solving the unsteady flow equations when supercritical flows exist. This results when the form of the Jacobian coefficient matrix is slightly changed due to the need for two upstream boundary conditions and none at the downstream boundary. The dam-break flood forecasting model is constructed to

accommodate supercritical flow for either the entire channel reach or for only an upstream portion of the entire reach. The supercritical flow regime is assumed to be applicable throughout the duration of the flow.

Lateral Outflow (q).--Often in the case of dam-break floods where the extremely high flows inundate considerable portions of channel overbank or valley bottom, a measurable loss of flow volume occurs. This is due to infiltration into the relatively dry overbank material, detention storage losses, and sometimes short-circuiting of flows from the main valley into other drainage basins via canals or overtopping natural ridges separating the drainage basins. Such losses of flow may be taken into account via the term q in Eq. (20). An expression describing the loss is given by the following:

$$q_m = -0.00458\ V_L\ P/(L\ \overline{T}) \quad \ldots\ldots\ldots\ldots\ldots\ldots\ldots\ldots \quad (44)$$

in which V_L is the outflow volume (acre-ft) from the reservoir; P is the volume loss ratio; L is the length (mi) of downstream channel through which the loss occurs; and $\overline{T}$ is the average duration (hr) of the flood wave throughout the reach length L; and q_m is the maximum lateral outflow (cfs/ft) occurring along the reach L throughout the duration of flow. The mean lateral outflow is proportioned in time and distance along the reach L such that $q_i^j=0$ when $Q_i^j=Q_i^1$ and $q_i^j=q_m$ when $Q_i^j=Q_{max_i}$. Thus:

$$q_i^j = \frac{(Q_i^j-Q_i^1)}{(Q_{max_i}-Q_i^1)}\ q_m \quad \ldots\ldots\ldots\ldots\ldots\ldots\ldots\ldots\ldots \quad (45)$$

where Q_i^1 is the initial flow and Q_{max_i} is the estimated maximum flow at each node determined a priori according to an exponential attenuation of the peak flow at the dam. The parameter P may vary from only a few percent to more than 30 depending on the conditions of the downstream valley.

Selection of Δt and Δx.--Rapidly rising hydrographs such as the dam-break outflow hydrograph can cause computational problems (instability and non-convergence) when applied to numerical approximations of the unsteady flow equations. This is the case even when an implicit, non-linear finite difference solution technique is used. However, the computational problems can be overcome by proper selection of time step (Δt) size and the distance step (Δx) size. During the limited testing of the model presented herein, two types of computational problems arose. First, if the time step were too large relative to the rate of increase of discharge during that time step, errors occurred in the computed water surface elevation in the vicinity of the wave front. These water surface elevations would tend to dip toward the channel bottom and quickly cause negative areas to be computed which would then cause the computations to "blow up." Second, too large a time step would also cause the Newton-Raphson iteration to not converge.

The first computational problem is similar to that experienced by Cunge [1975]. Both of the computational problems were successfully treated by reducing the time step size by a factor of 0.5 whenever negative areas were computed or when a reasonable number of iterations were exceeded. With the reduced time step, the computations were repeated. If the same problems persisted, the time step was again halved and the computations repeated. Usually one or two reductions would be sufficient. The computational process was then advanced to the next time level by the original unreduced time step. Computations were initially begun with Δt time steps (hr) in the following range:

$$0.05\,\tau < \Delta t < 0.10\,\tau \quad \ldots\ldots\ldots\ldots\ldots\ldots\ldots\ldots \quad (46)$$

in which τ is the time (hr) to peak of the outflow hydrograph.

Distance steps (Δx) were selected in the following range:

$$0.1 \leq \Delta x \leq 1.5 \quad \ldots\ldots\ldots\ldots\ldots\ldots\ldots\ldots \quad (47)$$

where Δx is in miles. The dam-break hydrograph tends to be a very peaked-type of hydrograph and as such tends to dampen and flatten out as it advances downstream. For this reason, smaller values of Δx were selected immediately downstream of the dam with a gradual increase in size at greater distances downstream of the dam. Also, the smaller values of Δx were associated with the smaller values of τ. This methodology of selecting Δx and Δt values follows the guidelines set forth in an analysis made by Fread [1974a] of the numerical properties of the four-point implicit solution of the unsteady flow equations.

Unlike the computational stability problem associated with explicit finite difference solutions, the implicit solution only has problems associated with the steep portion of the rising hydrograph in the vicinity of the wave front and in regions of the channel immediately downstream of the dam. Since the flood wave dampens out as it moves downstream, the computational problems tend to vanish. This feature of the dam-break wave can be taken advantage of with the implicit solution procedure used herein to develop an efficient computational procedure. This consists of increasing the Δt time step at an increasing rate as the computations advance in time. The following scheme is used:

$$\Delta t = \Delta t_o \qquad t \leq \tau \quad \ldots\ldots\ldots\ldots \quad (48)$$

$$\Delta t = 1.005\,\Delta t' \qquad \tau < t \leq 2\tau \quad \ldots\ldots\ldots\ldots \quad (49)$$

$$\Delta t = 1.010\,\Delta t' \qquad 2\tau < t \leq 3\tau \quad \ldots\ldots\ldots\ldots \quad (50)$$

$$\Delta t = 1.020\,\Delta t' \qquad 3\tau < t \leq 5\tau \quad \ldots\ldots\ldots\ldots \quad (51)$$

$$\Delta t \leq 1.0 \qquad t > 0 \quad \ldots\ldots\ldots\ldots \quad (52)$$

where Δt_o is the initial time step, the prime superscript indicates the previous time step, and Δt, Δt_o, $\Delta t'$, t, and τ are expressed in hours.

Outflow Hydrograph via Dynamic Routing.--As mentioned earlier, an option provided in the dam-break flood forecasting model is the use of dynamic routing rather than storage routing to compute the reservoir outflow hydrograph. The dynamic routing is identical to the above description with the exception of boundary and initial conditions. The upstream boundary condition is a discharge hydrograph given by the following:

$$Q_1^{j+1} - I(t) = 0 \quad \ldots \quad (53)$$

where $I(t)$ is the known reservoir inflow hydrograph. The downstream boundary condition is a stage-discharge relation similar to Eq. (3), i.e.,

$$Q_N^{j+1} - c_1(h_N^{j+1} - h_b^{j+1})^{1.5} - c_2(h_N^{j+1} - h_b^{j+1})^{2.5} - Q_s = 0 \quad \ldots \quad (54)$$

in which h_b, c_1, and c_2 are defined respectively by Eqs. (1), (4), and (5), and Q_s is the spillway(s) discharge as previously defined. The initial conditions are:

$$Q_i^1 = I(t=0) \qquad i = 1, 2, \ldots N \quad \ldots \quad (55)$$

$$h_i^1 = h_o \qquad i = 1, 2, \ldots N \quad \ldots \quad (56)$$

where h_o is the elevation of the water surface at the dam site when failure commences. The reservoir dynamic routing procedure must contend with the lowering of the water surface elevation at the upstream boundary as the reservoir volume is depleted by the outflow through the breach. If this depth becomes small and approaches a value less than the normal depth, the computations become unstable. To avoid this computational problem, the upstream depth is constantly monitored; if it becomes less than a specified critical depth (d_c), the location of the upstream boundary condition is shifted downstream one node at a time until the depth at the node is greater than d_c.

DATA REQUIREMENTS

The dam-break flood forecasting model requires certain input data, the type and quantity of which were an important consideration in the development of the model. Model components were selected which required data which were easily obtained by the forecaster and which allowed the forecaster to determine the quantity of data to be used.

The data required for the breach component of the model consists of the following parameters:

(1) The time (τ), in hours, from the start of the breach until it reaches its final dimensions; this may range from a few minutes to a few hours; its a priori specification is estimated by the forecaster based on the type and condition of the dam; its specification for updating forecasts is based on reports from observers;

(2) The bottom width (b), in feet, of the breach; a priori specification of b may range from $0.5 \leq b/h_o \leq 1.0$ for well-constructed earth and rock-fill dams to a value of b approaching the total width of the dam for poorly constructed earth dams and masonry dams; b values for updating forecasts can be obtained from observational estimates;

(3) The side slope (z) of the breach; a priori estimation of z may range from $0 \leq z \leq 1$ for earth and rock-fill dams, while z=0 is appropriate for masonry dams; z values for updating can be obtained from observational estimates;

(4) The final elevation (h_{bm}), in feet, of breach bottom; this is usually assumed to be the bottom of the dam unless tailwater elevations are relatively high compared to h_o;

(5) The reservoir length (L_R), in miles; and

(6) The elevation (h_o), in feet, of the water surface when failure commences; unless otherwise observed, this is assumed to be the top of the dam.

The outflow component requires the following data if storage routing is selected: a table of reservoir surface areas (A_s), in acres, coincident with elevations (h_A), in feet. Surface areas at any elevation are linearly interpolated by the following interpolation formula:

$$K = K_i + \frac{(h-h_i)}{(h_{i+1}-h_i)} (K_{i+1}-K_i) \qquad h_i \leq h \leq h_{i+1} \quad \ldots\ldots\ldots \quad (57)$$

where K is any interpolated value of a function, K(h).

The downstream routing component requires the following data:

(1) NS, number of downstream locations at which cross-sectional properties are specified;

(2) M, number of values in table of cross-sectional properties related to elevation;

(3) xs, distance (mi) downstream of dam to location of specified cross-section;

(4) hs_m (where m=1,2,...M), elevations (ft) at which cross-sectional properties are specified;

(5) Bs_m (where m=1,2,...M), top width (ft) of active cross-sectional area;

(6) Bso_m (where m=1,2,...M), top width (ft) of inactive (off-channel storage) cross-sectional area;

(7) BO, average width (ft), and DO, average depth (ft) of cross-section below hs_1;

(8) n_m (where m=1,2,...M), Manning roughness coefficient;

(9) k, expansion-contraction coefficient; and

(10) Dxm, minimum Δx distance between computational nodes (cross-sectional areas).

Items (4)-(7) are specified for each of the NS cross-sectional locations. Items (8)-(10) are specified for the (NS-1) reaches between the NS cross-sections.

The As_m (m=2,3,...M) values are computed from the following trapezoidal approximation after As_1 is computed as BO x DO:

$$As_m = As_{m-1} + \left(\frac{Bs_m + Bs_{m-1}}{2}\right)(hs_m - hs_{m-1}) \qquad m = 2, 3, \ldots M \quad . \quad . \quad . \quad (58)$$

Additional cross-sections are computed via a linear interpolation equation similar to Eq. (57) such that the minimum distance between cross-sections is less than or equal to the specified Dxm values. This feature enables only a minimum of cross-sectional data to be specified by the forecaster according to such criteria as data availability, data variation, etc. The cross-sectional data may be extracted from cross-sectional surveys or Geological Survey quadrangle maps, 7-1/2' series, scale 1:24000.

An option in the dam-break flood forecasting model is to specify NS surface areas (SA_m) rather than top widths. The surface areas may be obtained via planimetering around a given contour of the quadrangle maps. The surface areas are converted to top widths within the model.

Additional data required are:

(1) The initial steady discharge QOD (cfs) at the downstream boundary;

(2) The estimated maximum discharge QMAXD (cfs) at the downstream boundary; if this is entered as zero, the model estimates it via an exponential attenuation of the maximum outflow discharge;

(3) The maximum lateral outflow q_m (ft^2/sec) due to infiltration, detention, or short-circuiting losses as computed by Eq. (44); and

(4) The initial Δt time step size (hr).

If the dynamic routing option is selected for computing the outflow hydrograph, a similar type of data as used for the downstream routing component is required.

MODEL TESTING

Teton Dam

The dam-break flood forecasting model was applied to the recent failure of the Teton Dam, a typical earth-fill dam, 305 feet high, with a 3,000-foot long crest located on the Teton River in southeastern Idaho. The dam failed on June 5, 1976, killing 11 people, making 25,000 homeless, and inflicting about $400 million in damages to the Teton-Snake River Valley downstream of the Teton Dam. The inundated area is shown in Fig. 2. Observations were available on the approximate development sequence of the breach, the temporal description of the reservoir storage depletion, typical cross-sections and estimates of the Manning roughness coefficient for sections of the downstream valley approximately every 5 miles, indirect peak discharge measurements at three sites, and a continuous discharge hydrograph at a location about 60 miles downstream of the dam, flood peak travel times, and flood peak elevations. The data were made available by the Geological Survey in an unpublished report [Ray, et al., 1977].

The time of failure (τ) was estimated to be in the range of 0.5 to 1.5 hours. The following breach parameter values were used: τ = 1.5 hours, b = 150 feet, z = 0, h_{bm} = 0.0 feet, L_R = 17.0 miles, h_o = 261.5 feet. Cross-sectional properties at 12 locations along a 60-mile reach of the Teton-Snake River Valley below the dam were used. The downstream valley consisted of a narrow canyon (approximately 1,000 feet wide) for the first 5 miles and a wide valley which was inundated to a width of approximately 9.0 miles. Manning n values ranging from 0.028 to 0.047 were provided from field estimates by Geological Survey personnel. Minimum Δx values were gradually increased from 0.5 mile near the dam to 1.5 miles near the downstream boundary at the Shelly gaging station (valley mile 59.5 downstream

from dam). The reservoir surface area-elevation values were obtained from Geological Survey quadrangle maps. Additional input data included the following:

(1) QOD = 13,000 cfs;

(2) QMAXD = 65,000 cfs;

(3) $q_m = -0.30$ ft^2/sec, computed from Eq. (44) using P = 0.25, V_L = 240,000 acre-feet, L = 59.5 miles, and $\overline{T}$ = 15 hours; and

(4) $\Delta t_o = 0.125$ hour.

The reservoir storage routing option was used to generate the outflow hydrograph shown in Fig. 2. A comparison of the outflow hydrograph computed by the reservoir dynamic routing with that of the storage routing option is shown in Fig. 3. The difference is quite small; the peak of the storage routing is 4 percent greater than the dynamic routing while the rising limb and recessions of the outflow hydrograph produced by both routing techniques are almost identical.

The temporal variation of the computed outflow volume is shown in Fig. 4 along with the observed values. There is an average absolute difference of 2.7 percent between the observed and computed values.

The observed peak discharges obtained downstream from the Teton Dam by indirect measurements after the flood at miles 8.5, 43.0, and 59.5 are shown in Fig. 5. Most apparent in this figure is the extreme attenuation of the hydrograph peak. The computed hydrograph peaks are also shown in Fig. 5 for two cases. In one, the field estimated n values and an assumed q_m of 0.0 are used. In the other, the estimated n values were adjusted so that observed and computed flood peak travel times best coincided, and the lateral outflow (q_m) was computed from Eq. (44). The percentage loss parameter (P) was determined by comparison of the observed outflow volume from the reservoir and the volume of the observed hydrograph at the downstream boundary. The average absolute difference between the observed and computed peak discharges (using adjusted n values and a q_m value of -0.30 ft^2/sec) is 4.8 percent. The extensive attenuation of the observed hydrograph is simulated correctly by the model for both cases. This is due to the fact that valley storage is the significant cause of the attenuation and the cross-sectional areas appropriately describe this important characteristic of the downstream valley.

The cross-sectional areas were proportioned into active cross-sectional area (A) and inactive cross-sectional area (A_o) such that the maximum width of active cross-sectional area was about 2 miles. An attempt was made to model the flood using only active cross-sectional area. This required a very large adjustment (increase) of the estimated n values to simulate the correct flood travel time. Although the computed peak discharges were similar to those shown in

Fig. 5, the flood peak elevations were much too high. It was therefore concluded that an appropriate one-dimensional representation of the downstream flood phenomena included a maximum flow width of 2 miles and off-channel storage wherein the velocity was negligible relative to that in the active flow area.

An a priori selection of the breach parameters (τ and b) cause the greatest uncertainty in forecasting dam-break flood waves. The sensitivity of downstream discharges to reasonable variations in τ and b for the Teton Dam are shown in Fig. 6. Although there are large differences in the peak discharges near the dam, these become rather insignificant at locations more than about 15 miles downstream. The tendency for extreme attenuation of dam-break flood waves is accentuated in the case of the Teton Dam due to the existence of the very wide and flat valley, the bounds of which are apparent by the inundated area shown in Fig. 2. If the narrow canyon extended downstream all the way to Shelly, the differences in peak discharges would not have been damped-out to the extent shown in Fig. 6. Simulations of this type of downstream condition indicated that the upstream differences were more persistant at downstream locations. The differences at Shelly for the case of the canyon extension were about 94,000 cfs while those for the actual downstream valley were about 5,000 cfs as shown in Fig. 6.

A profile of the observed peak flood elevations downstream of the Teton Dam is shown in Fig. 7, along with the computed elevations using adjusted n values and $q_m = -.30$ ft^2/sec. The average absolute error is 1.5 feet while the average arithmetic error is only -0.2 foot.

The computed flood peak travel times are shown in Fig. 8 for the simulation using the original estimated n values and the adjusted n values. The latter was achieved through trial-and-error adjustments of n to best match the observed travel times. The final adjusted n values were about 7 percent less than the original estimates. Sensitivities of the computed peak stages, discharges, and travel times to changes in the Manning n were investigated for the Teton application. A 20-percent change in the Manning n values produced the following changes at the downstream boundary (Shelly):

(1) 0.5 foot in computed peak water surface elevations or about 2 percent of the maximum depth of flow;

(2) 15.7 percent deviation of the computed peak discharge;

(3) 0.8 percent change in total attenuation of peak discharge incurred in the 60-mile reach from the Teton Dam to Shelly; and

(4) 14.6 percent change in flood peak travel time.

These results indicate that the Manning n has a significant effect on the travel time but a very minor effect on the total transformation of the shape and magnitude of the dam-break flood wave as it advances through this 60-mile reach of the Teton-Snake River Valley.

A typical simulation of the Teton application involved 78 Δx reaches, 55 hours of prototype time, use of the reservoir storage routing option for computing the outflow hydrograph, and an initial time step (Δt_o) of 0.125 hours for the downstream dynamic routing component. Such a simulation run required only 14 seconds of CPU time on an IBM 360/195, i.e., the cost of a Teton Dam simulation run was approximately $2. An additional 2 seconds was required if the reservoir dynamic routing option were used.

Buffalo Creek Coal-Waste Dam

The dam-break flood forecasting model was also applied to the failure of the Buffalo-Creek coal-waste dam which collapsed on the Middle Fork, a tributary of Buffalo Creek (see Fig. 9) in southwestern West Virginia near Saunders. The dam failed very rapidly on February 26, 1972, and released about 500 acre-feet of impounded water into Buffalo Creek valley causing the most catostrophic flood in the state's history, with the loss of 118 lives, 500 homes, and property damage exceeding $50 million. Observations were available on the approximate development sequence of the breach, the time required to empty the reservoir, indirect peak discharge measurements at four sites, approximate flood peak travel times, and flood peak elevations [Davies, et al., 1972]. Cross-section and estimates of the Manning roughness coefficients were taken from a report on routing dam-break floods by McQuivey and Keefer [1975].

The time of failure was estimated to be in the range of 5 minutes and the reservoir took only 15 minutes to empty according to eyewitnesses reports. The following breach parameters were used: τ = 0.010 hours; b = 130 feet; z = 3.0, h_{bm} = 0.0 feet, L_R = 0.4 mile, h_o = 44.0 feet. Cross-sectional properties were specified for eight locations along the 15.7-mile reach from the coal-waste dam to below Man at the confluence of Buffalo Creek with the Guyandotte River as shown in Fig. 9. The downstream valley widened from the narrow width (approximately 100 ft) of Middle Fork to about 400-600 feet width of Buffalo Creek valley. Minimum Δx (Dxm) values were gradually increased from 0.2 mile near the dam to 0.4 mile near Man at the downstream boundary. The reservoir area-elevation values were obtained from Davies et al. [1972]. Additional input data included the following:

(1) QOD = 1,000 cfs;

(2) QMAXD = 30,000 cfs; and

(3) q_m = -0.08 ft^2/sec, computed from Eq. (44) using P = 0.25, V_L = 540 acre-feet, L = 15.7 miles, and $\overline{T}$ = 0.5 hour.

The 15.7-mile reach was divided into two reaches; one was approximately 4 miles long, in which the very steep channel bottom slope (84 ft/mi) produced supercritical flows, and the second extended on downstream approximately 12 miles, with an average bottom slope of 40 feet per mile, in which subcritical flows prevailed. An initial time step (Δt_o) of 0.010 hour was used in the downstream subcritical reach. The computations were unstable when the supercritical reach was modeled using the same type of boundary conditions as used with subcritical flows. This computational problem was eliminated when the supercritical boundary conditions Eq. (34) and Eq. (42) were used.

The reservoir storage routing option was used to generate the outflow hydrograph shown in Fig. 9. The computations indicated the reservoir was drained of its contents in approximately 15 minutes, which agreed with the observed time to completely empty its contents. The indirect measurements of peak discharge at miles 1.1, 6.8, 12.1, and 15.7 downstream of the dam are shown in Fig. 10. Again, as in the Teton Dam flood, the flood peak is greatly attenuated as it advances downstream. Whereas the Teton flood peak was attenuated by a factor of 0.65 in the first 16 miles of which 11 miles included the wide, flat valley below the Teton Canyon, the Buffalo Creek flood was confined to a relatively narrow valley but was attenuated by a factor of 0.87 in the same distance. The attenuation of the Buffalo Creek flood was due to the much smaller volume of its outflow hydrograph compared with that of the Teton flood.

In Fig. 10, the computed discharges agree favorably with the observed. There are two curves of the computed peak discharge in Fig. 10, one is associated with n values of 0.040. In the former, the n values are representative of field estimates while the latter results from adjustments in the n values such that computed flood travel times compare favorably with the observed. (Comparison of computed flood travel times with the observed are shown in Fig. 11 for estimated n values and for the final adjusted n values.) It should be noted that the two computed curves in Fig. 10 are not significantly different although the n values differ by a factor of 1.75. Again, as the Teton application, the n values influence the time of travel much more than the peak discharge. The large adjusted n values appear to be appropriate for dam-break waves in the near vicinity of the breached dam where flows are highly turbulent.

A profile of the observed peak flood elevations downstream of the Buffalo Creek coal-waste dam is shown in Fig. 12, along with the computed elevations using adjusted n values. The average absolute error is 1.8 feet and the average arithmetic error is -0.9 foot.

Sensitivities of the computed downstream peak discharges to reasonable variations in the selection of breach parameters (τ, b, and z) are shown in Fig. 13. The resulting differences in the computed discharges diminish in the downstream direction. Like the Teton dam-break flood

wave, errors in forecasting the breach are damped-out as the flood advances downstream.

A typical simulation of the Buffalo Creek flood involved 63 Δx reaches, 3.6 hours of prototype time, use of the reservoir storage routing option, and initial time steps of 0.005 and 0.01 hour for the supercritical and subcritical downstream reaches, respectively. Computation time for a typical simulation run was 9 seconds (IBM 360/195).

SUMMARY AND CONCLUSIONS

A dam-break flood forecasting model is described and applied to two actual dam-break flood waves. The model consists of a breach component which utilizes simple parameters to provide a temporal and geometrical description of the breach. A second component computes the reservoir outflow hydrograph resulting from the breach via a broad-crested weir-flow approximation, which includes effects of submergence from downstream tailwater depths and corrections for approach velocities. Also, the effects of storage depletion and upstream inflows on the computed outflow hydrograph are accounted for via either storage or dynamic routing within the reservoir. The third component consists of a dynamic routing technique for determining the modifications to the dam-break flood wave as it advances through the downstream valley, including its travel time and resulting water surface elevations. The dynamic routing component is based on a weighted, four-point, non-linear finite difference solution of the one-dimensional equations of unsteady flow. Provisions are included for routing supercritical flows as well as subcritical flows.

Model data requirements are flexible, allowing minimal data input when it is not available while permitting extensive data to be used when appropriate.

The model was tested on two recent dam-break flood waves, the Teton Dam failure and the collapse of the Buffalo Creek coal-waste dam. Computed outflow volume through each breach coincided with the observed values in magnitude and timing. Observed peak discharges along the downstream valley were satisfactorily reproduced by the model in each case even though each flood wave was severely attenuated as it advanced downstream. The computed peak flood elevations were within an average of 1.5 to 1.8 feet of the observed maximum elevations. Flood peak travel times were used to determine the appropriate Manning n coefficients, since this characteristic of the flood wave was significantly more sensitive to the roughness parameter than either discharge or water surface elevation. The Teton simulation required very small adjustments of n, however, the Buffalo Creek simulation required the estimated n values to be increased by a factor of 1.75. Each application indicated an important lack of sensitivity of downstream discharge to errors in the forecast of the breach size and timing. Such errors produced

significant differences in the peak discharge in the vicinity of the dam; however, the differences were rapidly reduced as the wave advanced downstream. This feature of the dam-break wave is related to the extent of storage volume in the reservoir. As the volume increases significantly beyond that associated with the test cases of this paper, the attenuation is significantly reduced and discharge errors at the dam will be more persistant in the downstream direction.

Computational requirements of the model are quite feasible; CPU time (IBM) 360/195) was 0.004 second and 0.159 second per hour per mile of prototype dimensions for the Teton Dam and Buffalo Creek, respectively. The more abrupt and smaller Buffalo Creek wave required smaller Δt and Δx steps; however, total computation times (9 sec vs. 14 sec) were similar since the smaller wave attenuated to insignificant values in a shorter distance and in less time than the Teton flood wave.

APPENDIX I. REFERENCES

Amein, M., and C. S. Fang, 1970: Implicit flood routing in natural channels. Journ. Hydraul. Div., ASCE, 96, HY12, Dec., pp. 2481-2500.

Baltzer, R., and C. Lai, 1969: Computer simulation of unsteady flows in waterways. Journ. Hydraul. Div., ASCE, 94, HY4, July, pp. 1083-1117.

Brater, E., 1959: Hydraulics. Civil Engineering Handbook, edited by L. C. Urquhart, Sect. 4, McGraw-Hill Book Co., New York, pp. 4.44-4.60.

Chaudhry, Y. M., and D. N. Contractor, 1973: Application of the implicit method to surges in open channels. Water Resour. Res., 9, No. 6, Dec., pp. 1605-1612.

Cristofano, E. A., 1965: Method of computing rate for failure of earth fill dams. Bureau of Reclamation, Denver, Colo., April.

Cunge, J. A., 1975: Rapidly varying flow in power and pumping canals. Unsteady Flow in Open Channels, edited by K. Mahmood and V. Yevjevich, Vol. II, Chapt. 14, Water Resour. Pub., Ft. Collins, Colo., pp. 539-586.

Davies, W. E., J. F. Bailey, and D. B. Kelly, 1972: West Virginia's Buffalo Creek flood: a study of the hydrology and engineering geology. Geological Survey Circular 667, U.S. Geological Survey, 32 pp.

De Saint-Venant, Barré, 1871: Theory of unsteady water flow, with application to river floods and to propagation of tides in river channels. Acad. Sci. (Paris) Comptes rendus, 73, pp. 237-240.

Dressler, R. F., 1954: Comparison of theories and experiments for the hydraulic dam-break wave. Internat. Assoc. Sci. Pubs., 3, No. 38, pp. 319-328.

Fread, D. L., 1971: Discussion of implicit flood routing in natural channels. M. Amein and C. S. Fang, Journ. Hydraul. Div., ASCE, 97, HY7, July, pp. 1156-1159.

Fread, D. L., 1974a: Numerical properties of implicit four-point finite difference equations of unsteady flow. NOAA Tech. Memo. NWS HYDRO-18, U.S. Dept. of Commerce, NOAA, National Weather Service, 38 pp.

Fread, D. L., 1974b: Implicit dynamic routing of floods and surges in the Lower Mississippi. Presented at AGU Natl. Mtg, Wash., D.C., April, 26 pp.

Liggett, J., and J. A. Cunge, 1975: Numerical methods of solution of the unsteady flow equations. Unsteady Flow in Open Channels, edited by K. Mahmood and V. Yevjevich, Vol. I, Chapt. 4, Water Resour. Pub., Ft. Collins, Colo., pp. 89-182.

Martin, C. S., and J. J. Zovne, 1971: Finite-difference simulation of bore propagation. Journ. Hydraul. Div., ASCE, 97, HY7, July, pp. 993-1010.

McQuivey, R. S., and T. N. Keefer, 1976: Application of simple dam break routing model. Proceedings, 16th Congress, IAHR, San Paulo, Brazil, July 27-August 1, 1975, Vol. 2, pp. 315-324.

Preissmann, A., 1961: Propagation of translatory waves in channels and rivers. Paper presented at First Congress of French Assoc. for Computation, Grenoble, Sept. 14-16, Proceedings, AFCAL, pp. 433-442.

Ray, H. A., L. C. Kjelstrom, E. G. Crosthwaite, and W. H. Low, 1976: The flood in southeastern Idaho from the Teton Dam failure of June 5, 1976. Unpublished open file report, U.S. Geological Survey, Boise, Idaho.

Ré, R., 1946: A study of sudden water release from a body of water to canal by the graphical method. Houille Blanche (France), No. 3, pp. 181-187.

Ritter, A., 1892: The propagation of water waves. Ver. Deutsch Ingenieure Zeitschr. (Berlin), 36, Pt. 2, No. 33, pp. 947-954.

Sakkas, J. G., and T. Strelkoff, 1973: Dam break flood in a prismatic dry channel, Journ. Hydraul. Div., ASCE, 99, HY12, Dec., pp. 2195-2216.

Schocklitsch, A., 1917: On waves created by dam breaches. Akad. Wiss. (Vienna) Proc., 126, Pt. 2A, pp. 1489-1514.

Stoker, J. J., 1957: Water Waves, Inter-Science Pub., New York, pp. 333-341.

Strelkoff, T., 1970: Numerical solution of Saint-Venant equations. Journ. Hydraul. Div., ASCE, 96, HY1, Jan., pp. 223-252.

Su, S. T., and A. H. Barnes, 1970: Geometric and frictional effects on sudden releases. Journ. Hydraul. Div., ASCE, 96, HY11, Nov., pp. 2185-2200.

Terzidis, G., and T. Strelkoff, 1970: Computation of open channel surges and shocks. Journ. Hydraul. Div., ASCE, 96, HY12, Dec., pp. 2581-2610.

U.S. Army Corps of Engineers, 1960: Floods resulting from suddenly breached dams--conditions of minimum resistance, hydraulic model investigation. Misc. Paper 2-374, Report 1, WES, Feb., 176 pp.

U.S. Army Corps of Engineers, 1961: Floods resulting from suddenly breached dams--conditions of high resistance, hydraulic model investigation. Misc. Paper 2-374, Report 2, WES, Nov., 121 pp.

U.S. Army Corps of Engineers, 1975: National Program of Inspection of Dams, Vol. I-V, Dept. of the Army, Office of Chief of Engineers, Wash., D.C.

Venard, J. K., 1954: Elementary Fluid Mechanics, John Wiley and Sons, New York, pp. 312-325.

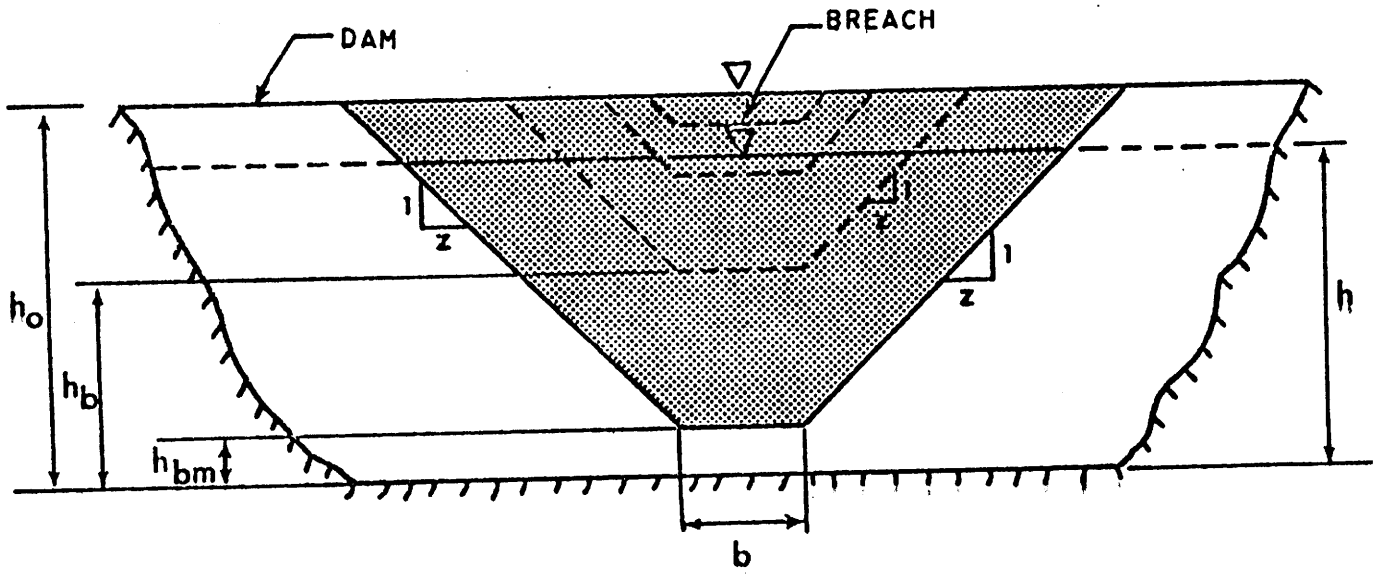

Fig. 1 – FRONT VIEW OF DAM SHOWING FORMATION OF BREACH

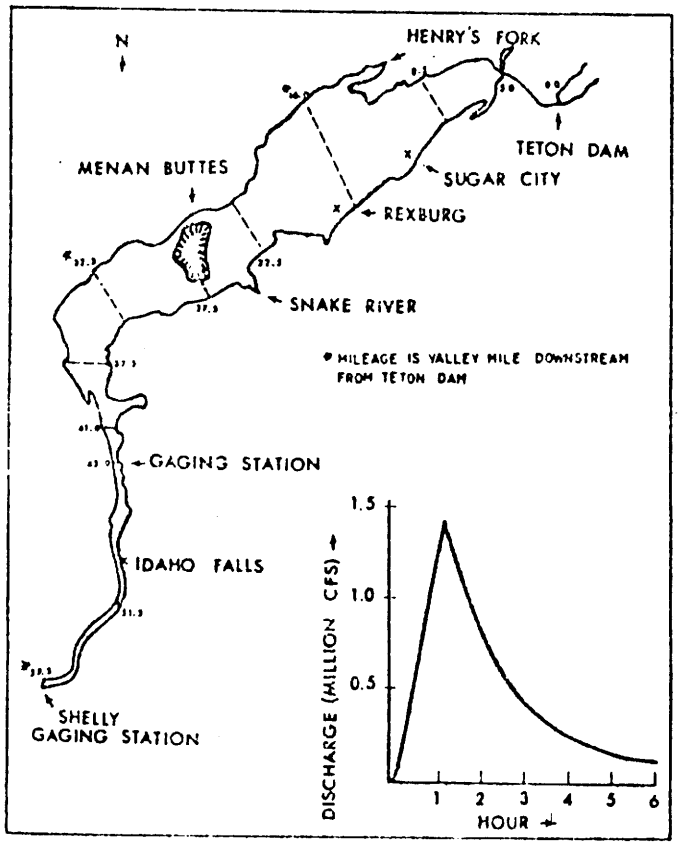

Fig. 2 – OUTFLOW HYDROGRAPH AND FLOODED AREA DOWNSTREAM OF TETON DAM

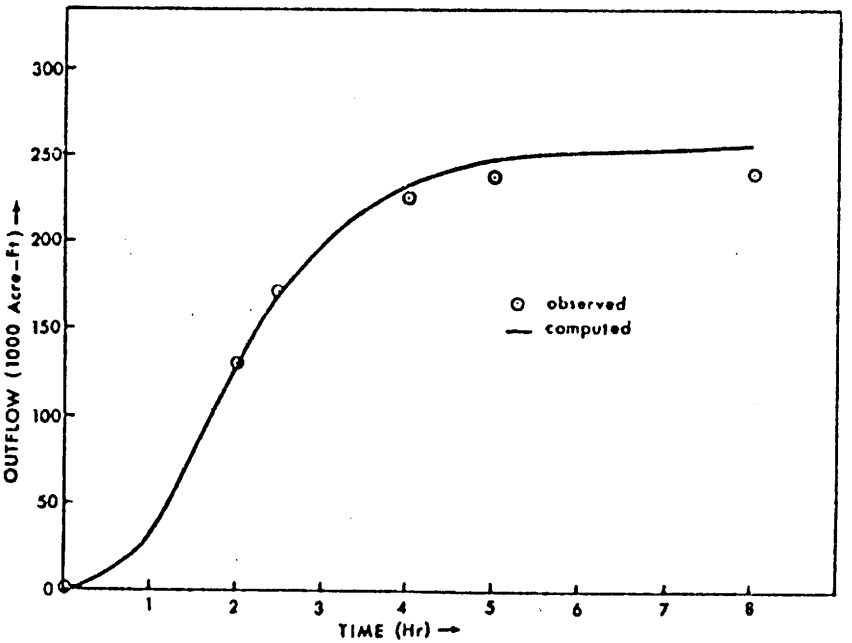

Fig. 3 – OUTFLOW VOLUME FROM TETON DAM

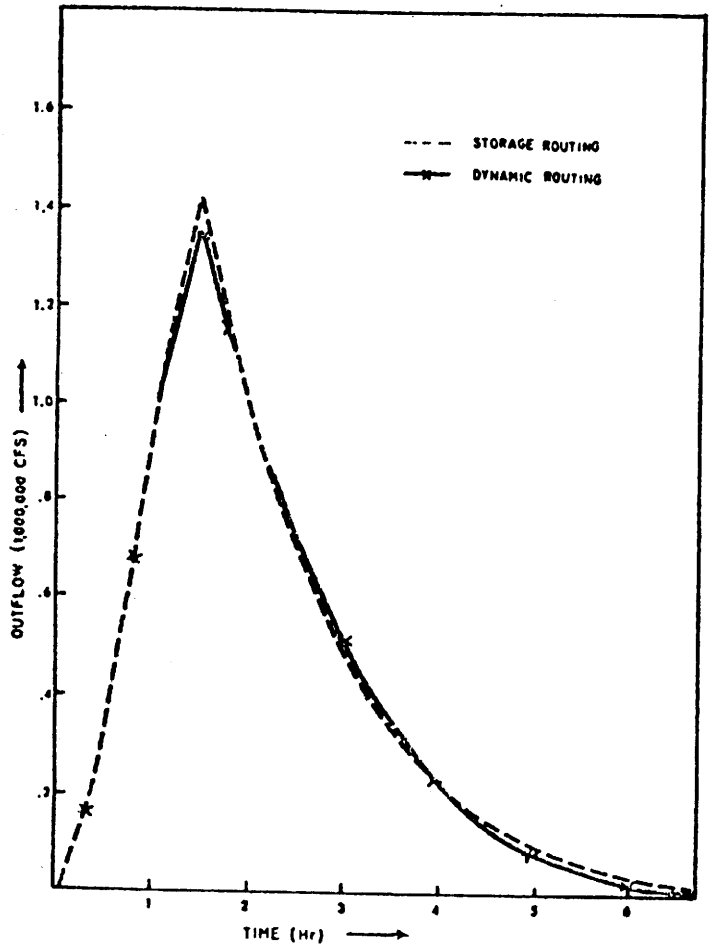

Fig. 4 – OUTFLOW HYDROGRAPH FROM TETON DAM FAILURE

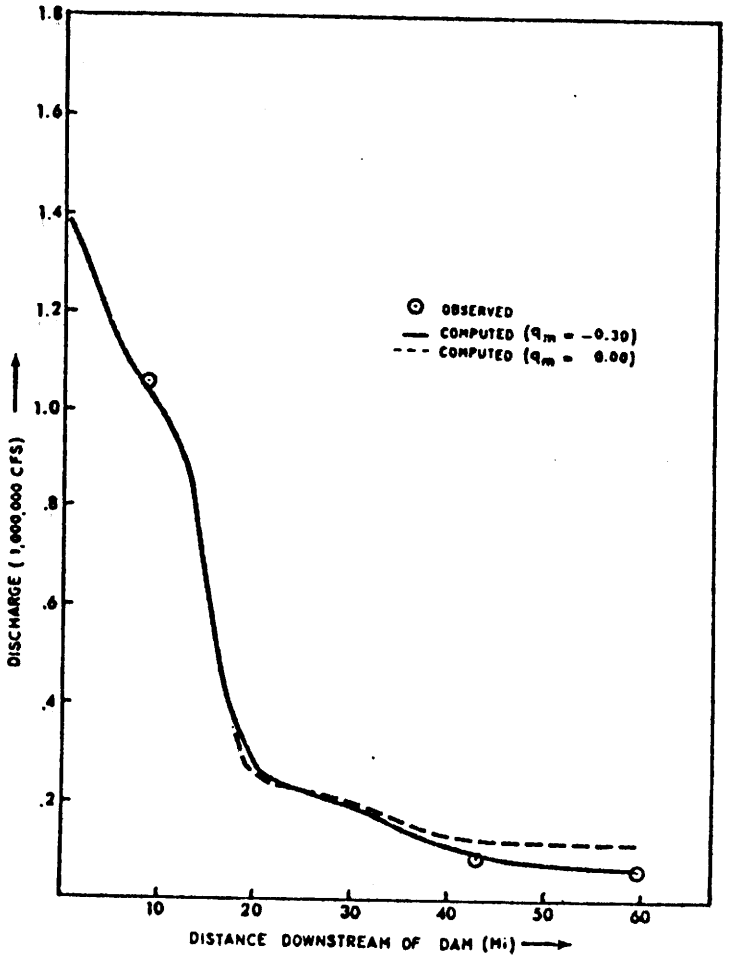

Fig. 5 – PROFILE OF PEAK DISCHARGE FROM TETON DAM FAILURE

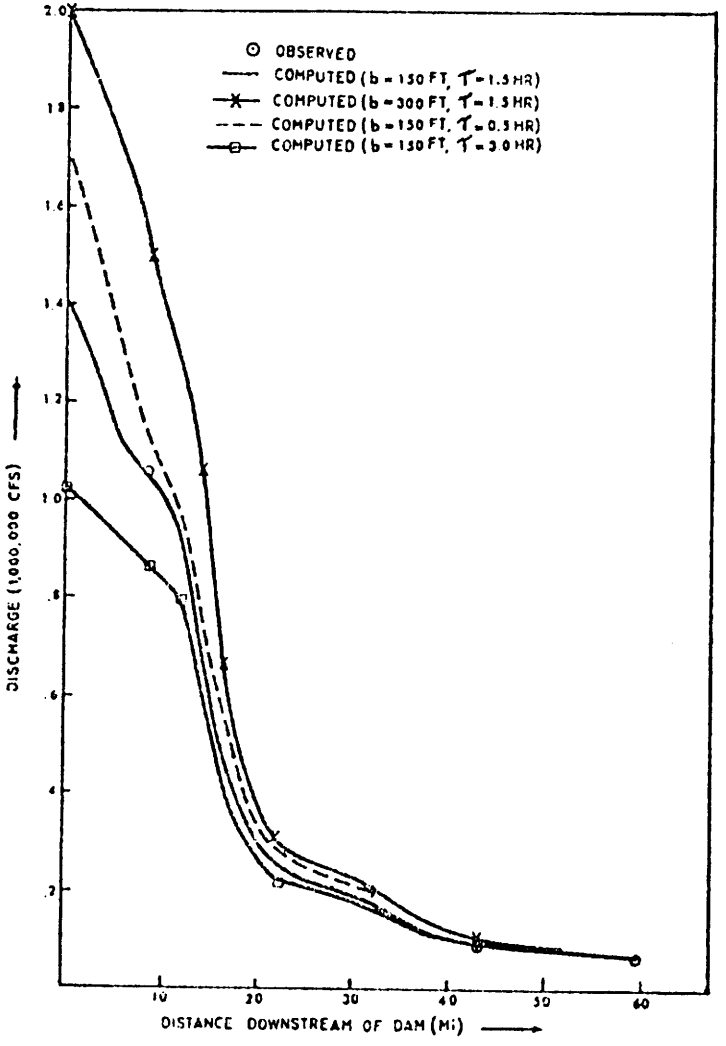

Fig. 6 — PROFILE OF PEAK DISCHARGE FROM TETON DAM FAILURE SHOWING SENSITIVITY OF VARIOUS INPUT PARAMETERS

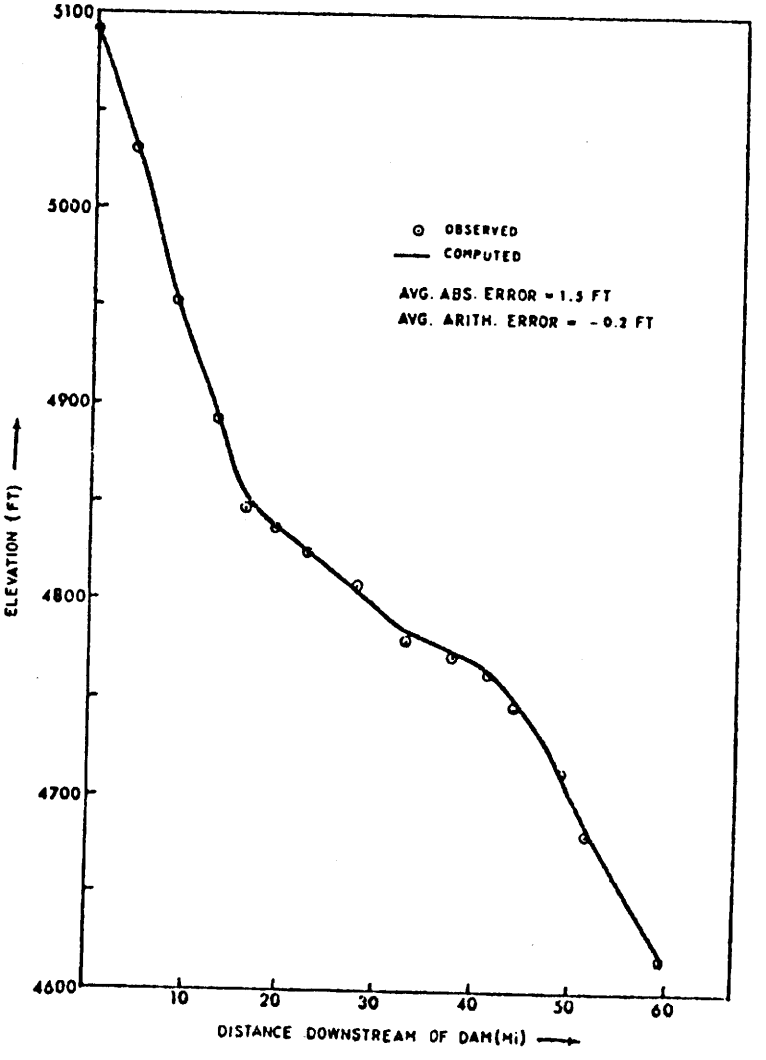

Fig. 7 — PROFILE OF PEAK FLOOD ELEVATION FROM TETON DAM FAILURE

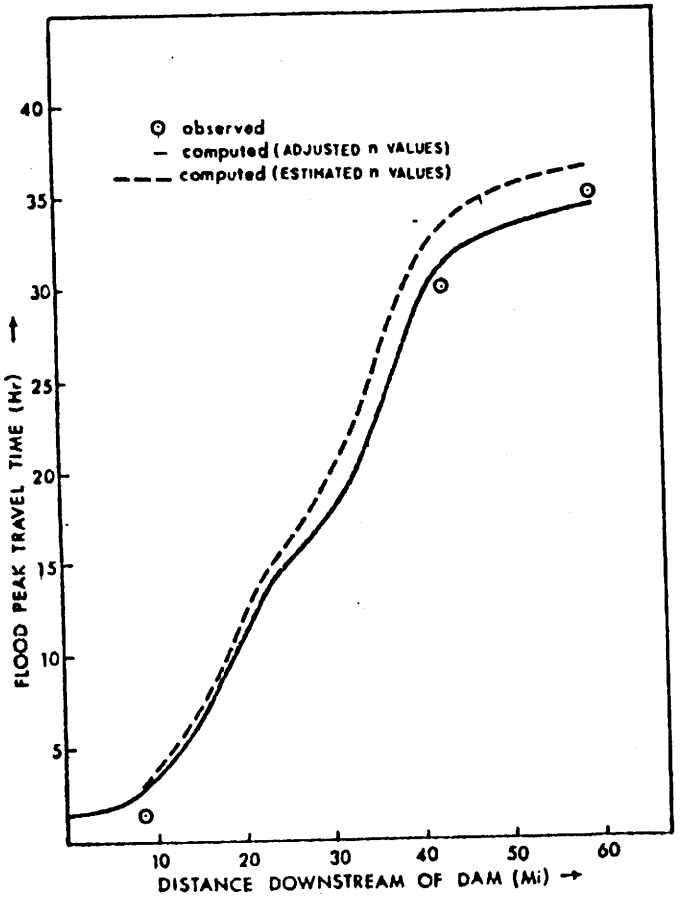

Fig. 8 — TRAVEL TIME OF FLOOD PEAK FROM TETON DAM FAILURE

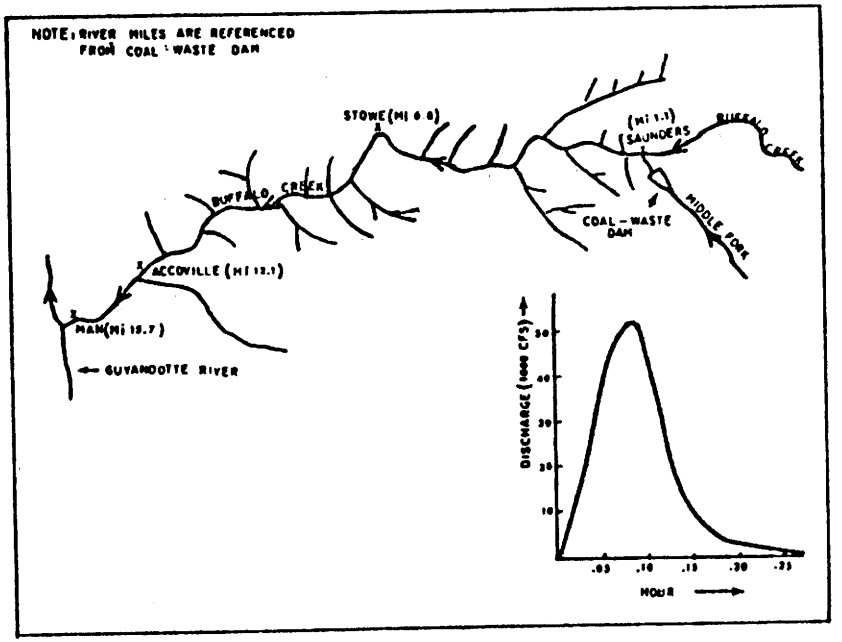

Fig. 9 — OUTFLOW HYDROGRAPH FROM COAL-WASTE DAM AND LOCATION PLAN OF BUFFALO CREEK

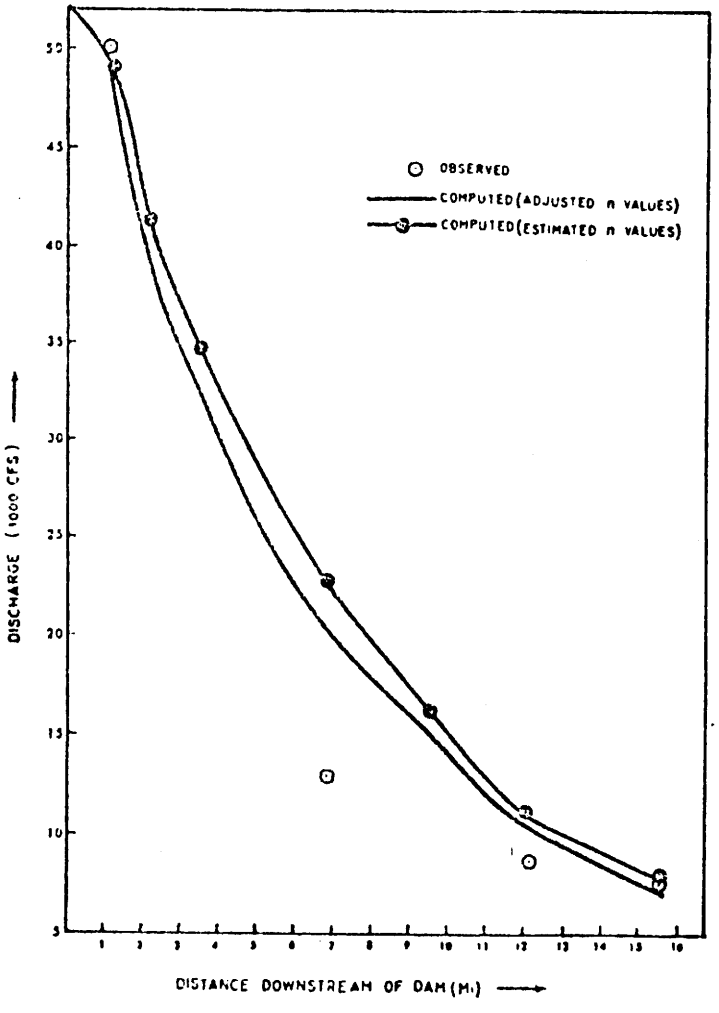

Fig. 10 — PROFILE OF PEAK DISCHARGE FROM BUFFALO CRK. FAILURE

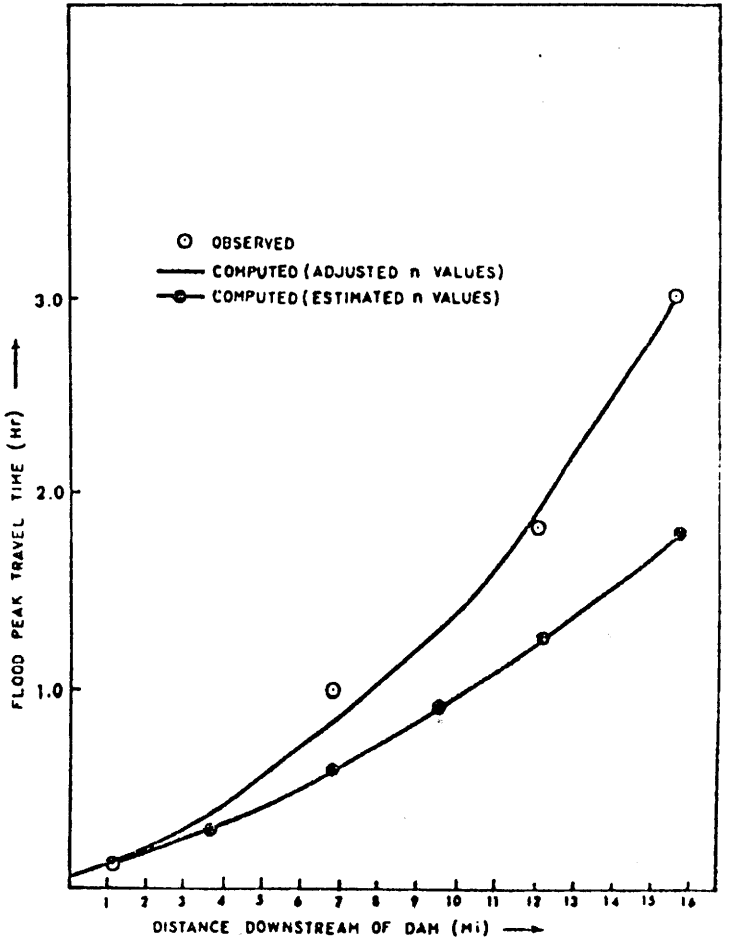

Fig. 11 — TRAVEL TIME OF FLOOD PEAK FROM BUFFALO CREEK FAILURE

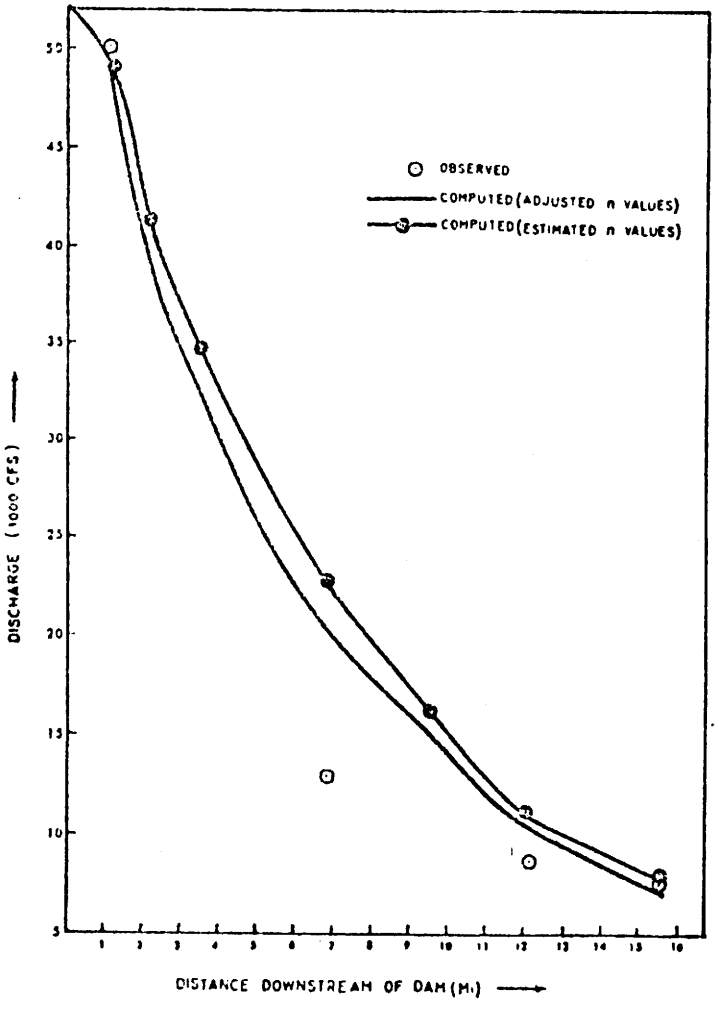

Fig. 10 — PROFILE OF PEAK DISCHARGE FROM BUFFALO CRK. FAILURE

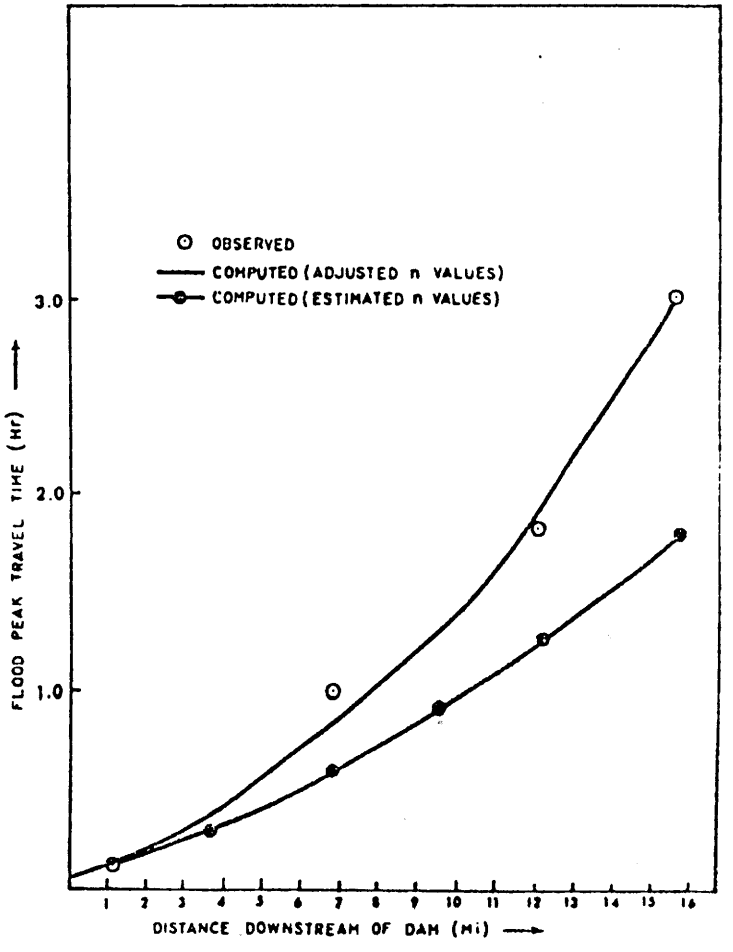

Fig. 11 — TRAVEL TIME OF FLOOD PEAK FROM BUFFALO CREEK FAILURE

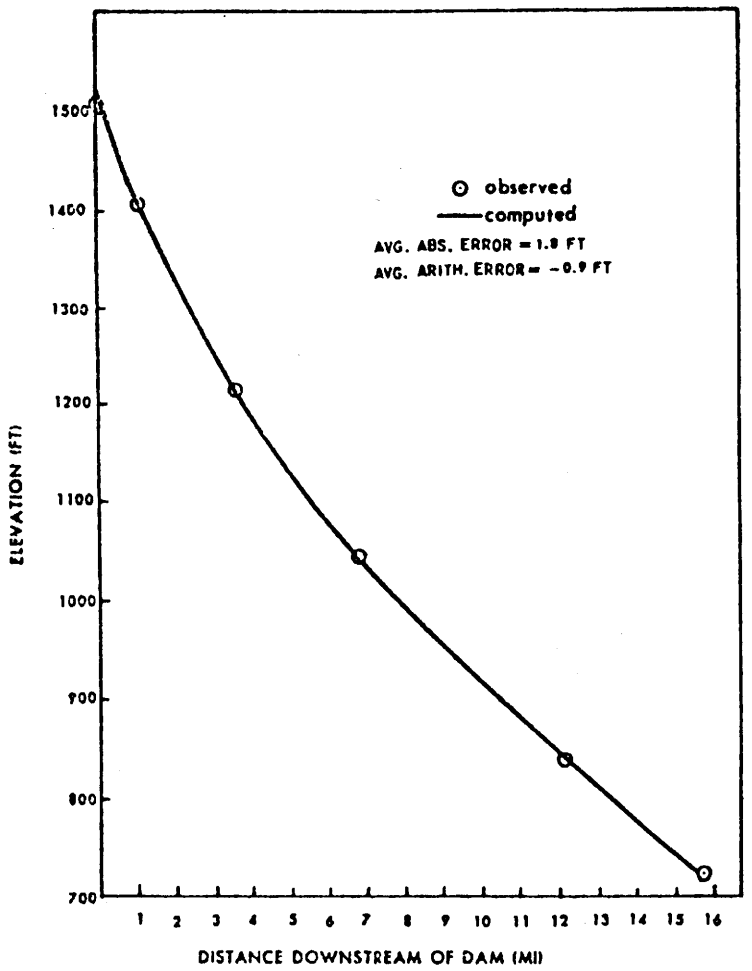

Fig. 12 – PROFILE OF PEAK FLOOD ELEVATION FROM BUFFALO CREEK FAILURE

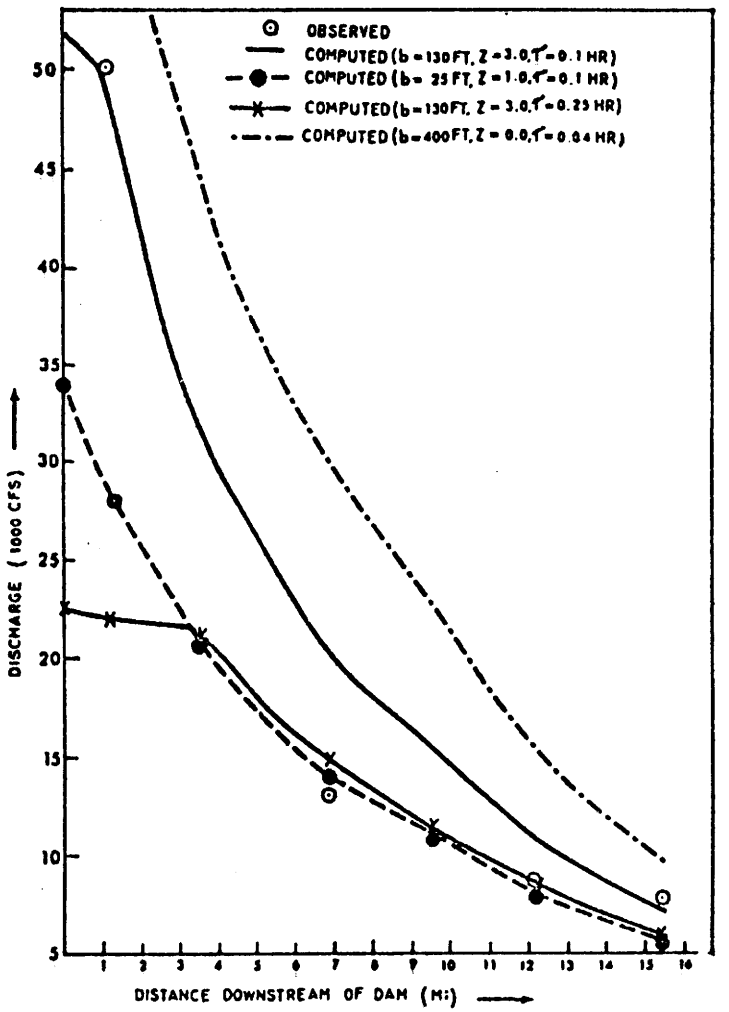

Fig. 13 – PROFILE OF PEAK DISCHARGE FROM BUFFALO CRK. FAILURE SHOWING SENSITIVITY OF VARIOUS INPUT PARAMETERS